Enhanced photothermoelectric detection in Co:BiCuSeO crystals with tunable Seebeck effect

FAN WANG,[1,2,5] **YANGYANG LV,**[1,2,5] **YANMING XU,**[1,2] **LIN CAO,**[1,2] **LIDA CHEN,**[1,3] **CHI ZHANG,**[1,3] **SHUHUA YAO,**[1,3,6] **JINLONG XU,**[1,4,7] **JIAN ZHOU,**[1,3] **AND YANBIN CHEN**[1,2]

[1]*National Laboratory of Solid State Microstructures, Nanjing University, Nanjing 210093, China*
[2]*Department of Physics, Nanjing University, Nanjing 210093, China*
[3]*Jiangsu Key Laboratory of Artificial Functional Materials & Department of Materials Science and Engineering, Nanjing University, Nanjing 210093, China*
[4]*School of Electronic Science and Engineering, Nanjing University, Nanjing 210093, China*
[5]*These authors contributed equally to this work*
[6]*shyao@nju.edu.cn*
[7]*longno.2@163.com*

Abstract: BiCuSeO is a widely-used thermoelectric material recently proved to be an appealing candidate for broadband photothermoelectric (PTE) detection. Developing a simple and scalable route for advancing PTE properties is therefore essential to explore the full potential of BiCuSeO. Here we systematically demonstrated that Co^{3+} atomic doping strategies in BiCuSeO single crystals (Co concentration of 1%, 2% and 4%) could modulate the Seebeck coefficient and thus strongly improve the performance of BiCuSeO PTE photodetectors across visible to infrared spectral regions. Benefiting from these strategies, a large enhancement on photovoltage responsivity is achieved and the response time of a 4% Co:BiCuSeO PTE photodetector is one order of magnitude faster than those in most of PTE photodetectors. Also, Co:BiCuSeO PTE photodetectors show good stability with changeless photoresponse after being exposed to air for three months. Therefore, the controllable atomic doping of BiCuSeO with tunable PTE properties as well as fast and broadband photodetection provides the feasibility for facilitating ongoing research toward PTE devices.

1. Introduction

Traditional photoelectric detectors based on photoconductive (PC) and photovoltaic (PV) effects are limited by the optical bandgap of the semiconductors therein, which usually operate within a narrow spectral range. To solve these problems, recent research on the photodetectors based on PTE effect has become increasingly popular [1]. The PTE effect consists of two processes: photo-thermal conversion and thermo-electric conversion. For photo-thermal conversion, one side of the PTE material absorbs photon energy to generate heat, and then a temperature difference (ΔT) is produced between the photon absorption side and the opposite one. In other words, there is a transverse temperature gradient established in the photodetector. For thermo-electric conversion, under the action of the temperature gradient, the charge carriers diffuse from the hot side to the cold one, thereby generating an electric potential difference (ΔU), which is namely the Seebeck effect ($\Delta U = S \times \Delta T$, where S is the Seebeck coefficient). Through above-mentioned physical processes, the operation of PTE photodetectors needs no external bias voltage and has no relationship with electron transition from valence to conduction bands, which are completely different from the traditional photoelectric detectors. Therefore, PTE photodetectors have two advantages over photoelectric detectors. One is the free of external bias that leads to no shot

noise and 1/f noise, where only Johnson-Nyquist noise affects the device performance [1–3]. The other is the free of electron transition, introducing a large spectral range of detection beyond the limitation of material bandgap [4].

The photoresponse of PTE photodetectors mainly depends on the Seebeck effect. In order to evaluate the efficiency of the thermoelectric conversion, the thermoelectric figure of merit ZT is defined as $ZT = S^2\sigma T/\kappa$, where σ is the electrical conductivity, κ being the thermal conductivity [5]. It can be concluded that employment of PTE material with a large σ can lead to a good conductivity, and a low κ is benefit to establish a large ΔT. If the material has a large S and a large ΔT, a great ΔU will be produced [6]. The possible route toward this goal has been verified by using two-dimensional nanomaterials [7–10], perovskites [11], traditional thermoelectric bulk materials [12–15], etc. For example, constructing PTE photodetectors with two-dimensional nanomaterials such as graphene. It realized high responsivity and fast response speed [7] owing to their strong electron-electron interaction and carrier multiplication process [16–18]. However, the very low saturation threshold of graphene restricts the detection operation within a low illumination power level. Only when the incident power is less than 20 μW, the photoresponse is in the linear region [19]. For perovskites, the poor long-term stability in ambient environment is a challenging problem that limits their applications. The photoresponse of perovskites PTE photodetectors is gradually deteriorating with increasing illumination time [20]. As far as the PTE photodetectors based on traditionally thermoelectric materials (such as $SrTiO_3$ and SnSe) are concerned, they usually have wide linear response region even under high laser power, while their low responsivity and long response time remain a primary bottleneck for further implementation [12,14]. Therefore, looking for high responsivity, fast response speed and stable thermoelectric material is of great significance to next-generation PTE photodetectors.

Recent study has shown BiCuSeO crystal is an excellent thermoelectric material with a large Seebeck coefficient of up to 349 μV/K at room temperature and a high ZT value of 0.6 at 873 K [21,22]. Besides, as an oxide, BiCuSeO has good thermal stability in the medium temperature range (300-900 K) [23]. BiCuSeO has been considered to construct PTE photodetectors by using its light-induced transverse thermoelectric (LITT) effect [24–28]. However, the reported responsivity is only around 0.012 V/W at 532 nm in BiCuSeO film with 120 nm thickness, due to the small temperature gradient between the top and bottom surfaces of the thin film. Further improvement of the performance of BiCuSeO photodetector is therefore urgent, especially on how to maximize its PTE effect to improve the responsivity.

In this article, we demonstrated that slightly Co^{3+} doping in BiCuSeO single crystal can increase Seebeck coefficient without inducing structure distortion, which thus largely enhances its PTE detection performance. The characteristics of Co:BiCuSeO with several doping concentrations (Co concentration of 1%, 2% and 4%) in PTE photodetectors have been systematically studied in the visible-near infrared range (444-1600 nm). The 4% Co:BiCuSeO exhibits the highest responsivity (0.48 V/W at 808 nm), as well as other outstanding performances, such as fast response speed (195 ms), high saturation power (without saturation even up to 2 mW) and excellent stability (more than three months). Such atomic doping strategy may promote the development of PTE materials and devices.

2. Experimental results and discussions

The pristine and Co:BiCuSeO (Co concentrations of 1%, 2% and 4%) single crystals were all grown by the chemical vapor transport (CVT) method. Firstly, the powders of Bi, Bi_2O_3, Cu, Se, and Co were heated in a sealed vacuum quartz tube at 700°C for 7 days, and the polycrystalline powders were synthesized by the solid-state reaction method. Secondly, the synthesized Co:BiCuSeO polycrystalline powder and 10 mg/ml of I_2 were mixed into an evacuated quartz ampoule. Thirdly, the evacuated quartz ampoule was placed into a two-zone furnace with a temperature distribution of 600-700°C to grow crystals. Finally, after more than 10 days,

millimeter-sized flake BiCuSeO crystals with several Co-doped concentrations (0, 1%, 2% and 4%) were obtained, respectively, as presented in Fig. 1(a) inset. Figure 1(a) is the lattice structure of Co:BiCuSeO single crystals and the inset is the optical micrograph of the crystals. The pristine BiCuSeO single crystal belongs to tetragonal system with space group of P4/nmm. Due to Co doping, Co atoms can effectively compensate the Bi-deficiency which naturally exists in pristine BiCuSeO crystals [29]. Figure 1(b) is the XRD of as grown pristine BiCuSeO and Co:BiCuSeO (Co concentrations of 1%, 2% and 4%) single crystals showing the [00*L*]-reflections, which verifies the *ab*-plane being the exposed surface. It can be seen from XRD that slight Co doping will not significantly change the crystal structure. As shown in Fig. 1(c), the absorption spectra of these single crystals were measured with an ultraviolet-visible-near-infrared spectrophotometer (PerkinElmer LAMBDA950). Please note that there is almost no change at the broadband absorption spectra between the Co doping and pristine BiCuSeO, confirming that such slight Co doping level does not introduce defect states and structure distortions. Besides, from the absorption spectra, the optical bandgap of Co:BiCuSeO is determined to be 0.8 eV. For Seebeck coefficient measurement, the as-grown crystals were fixed on an iron block using two pieces of unconnected thermally conductive adhesives. A ceramic heater was placed in one of the thermally conductive adhesives to generate a temperature gradient along the length of the sample. Then conductive silver paste was coated both the ends of the sample as electrodes to measure the voltage. In the experiment, the temperature variation at both ends of the sample was determined by a Fotric 228 Thermal Imager, and the generated voltage was detected by a Keithley 2450 SourceMeter. For comparison, the results for the series of Co doping are plotted in Fig. 1(d). Increasing the Co concertation leads to higher Seebeck coefficient since Co atoms can effectively compensate the Bi-deficiency which naturally exists in pristine BiCuSeO crystals [29]. The 4% Co concentration has the largest Seebeck coefficient of 962 µV/K, nearly three times larger than 332 µV/K of pristine BiCuSeO crystal, indicating a more potential PTE application.

This Co-doping engineering in BiCuSeO single crystals makes them feasible for the PTE photodetector. Therefore, photodetectors based on Co:BiCuSeO and pristine BiCuSeO have been fabricated on SiO_2 substrate in order to investigate the effect of doping. As schematically shown in Fig. 2(a), with patterning silver electrodes on both ends of the samples, the channel of the photodetectors was 0.8 mm in length and 1 mm in width. During the experiment, the laser beams were focused on the interface between the crystals and the left silver electrodes. The SourceMeter was connected the two electrodes to measure the photovoltage signals. Figure 2(b) shows the recorded current-voltage (*I-V*) curves in dark environment. The standard linear curves within a wide bias voltage range from -10 to 10 mV, indicating a good Ohmic contact between the crystal and the silver electrodes. The linear Ohmic contact suggests the absence of the PV effect, because the PV effect requires a built-in electric field in the detectors. As we mentioned in our previous study [29], one can see that the resistance of the crystal increases with doping level and the carrier concentrations of un-doped, 1%, 2% and 4% Co:BiCuSeO are 251.1×10^{18}, 134.6×10^{18}, 4.2×10^{18} and 1.1×10^{18} cm^{-3}, respectively at room temperature. Quantitatively, the resistance of the 4% Co:BiCuSeO crystal reaches to 14.7 kΩ, while that of pristine one is only 1.1 kΩ. Figure 2(c) compares the *I-V* curves of 4% Co:BiCuSeO PTE photodetector with laser illumination (808 nm wavelength, 1 mW power) and in dark. The laser illuminates at the interface between the electrode and the single crystal on the left (L-interface) and right (R-interface) sides. It is important to note that the three *I-V* curves are parallel to each other, indicating that the laser illumination has no effect on the resistance of the crystals. Therefore, the PC effect of the photodetectors also can be ruled out. Compared with that in dark, the *I-V* curve for L-interface (R-interface) obviously moves down (up) along y-axis, which is the typical characteristic of the PTE effect [30]. As illustrated in Fig. 2(d), the laser irradiation at different positions of the photodetector generates different photovoltage. The direction of the photovoltage on the L-interface is opposite to that on the R-interface. The photovoltage reaches maximum
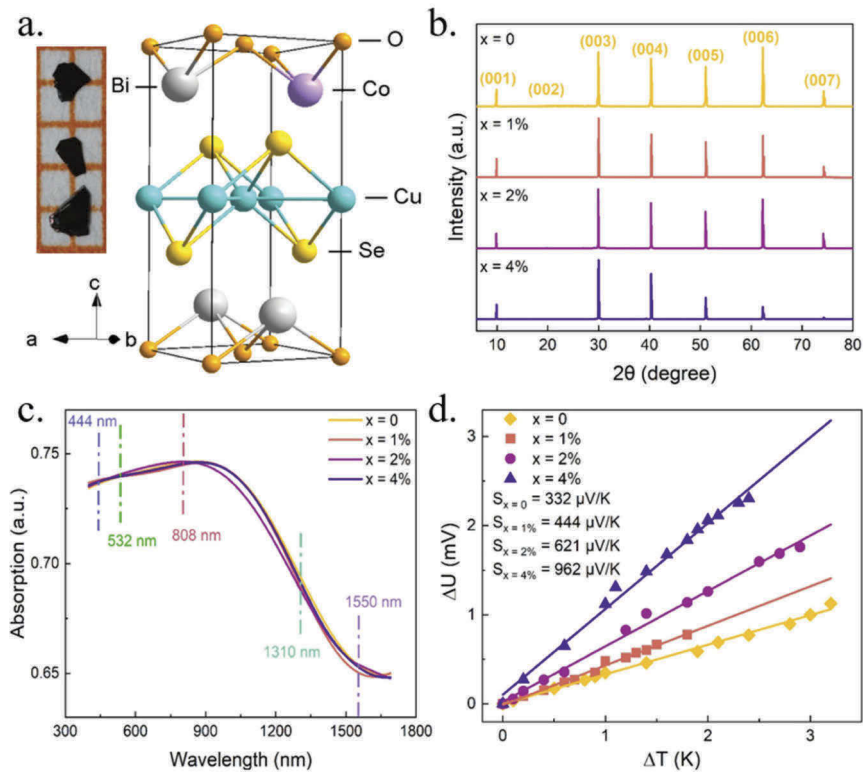
Fig. 1. (a) Lattice structure of Co:BiCuSeO crystals. Inset: Optical micrograph of as-grown Co:BiCuSeO single crystals. (b) XRD of pristine and Co:BiCuSeO crystals. (c) Absorption spectra of pristine and Co:BiCuSeO crystals. (d) Seebeck coefficient of pristine and Co:BiCuSeO crystals.

at L-interface, decreasing to zero with the laser gradually close to the middle of the channel, and turning to negative when moving the laser to R-interface. This phenomenon is a typical characteristic of PTE effect which is distinct from PV or PC effect. The reason is the opposite direction of the temperature gradient generated by the laser illumination between the L- and R-interface Meanwhile, the temperature difference between both crystal sides is maximum (zero) at the two interfaces (middle of the channel). It is noteworthy that 4% Co:BiCuSeO crystal shows the best photoresponse within the four samples, which can be naturally understood as it has the largest Seebeck coefficient therein (see Fig. 1(f)).

We further explored the photoresponse behavior of the processed photodetectors in deep at zero source-drain bias and at room temperature. A series of laser in visible (444 and 532 nm) and near-infrared (808, 1310 and 1550 nm) spectral regions were used as the light sources. The corresponding spot diameters on the samples were 0.17, 0.17, 0.25, 0.15 and 0.15 mm, respectively, measured by the scanning knife-edge method. Figure 3 summarizes the photoresponse comparisons among the three Co-doping and the pristine BiCuSeO. The time-dependent photovoltage measurements for the five wavelengths were spliced in Fig. 3(a), with illumination power all fixed at 1 mW. Clearly, the Co-doping samples exhibit superior photovoltage response overwhelming the pristine BiCuSeO in the whole tested wavelength range. In these results, the photovoltage for 4% Co:BiCuSeO reaches 0.45 mV at 808 nm, which is beyond four times higher than that of the undoped one (0.1 mV). In Fig. 3(b), all the photodetectors showcase whole linear relationship with illumination power, which can
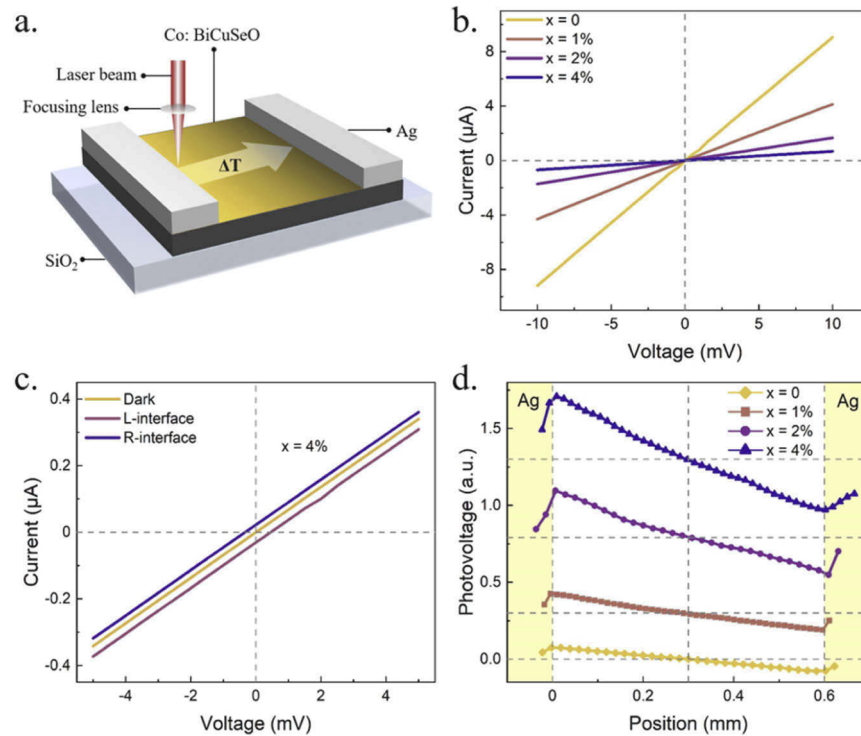
Fig. 2. (a) Schematic of Co:BiCuSeO-Ag contact device used for PTE photodetection. (b) Current-voltage curves of Co:BiCuSeO in dark. (c) Current-voltage curves of 4% Co:BiCuSeO in dark (yellow line) and under 808 nm, 1 mW laser illumination at the L-interface (red line) and R-interface (purple line). (d) Position-dependent photovoltage response under 808 nm, 1 mW illumination with a focused light spot of 0.25 mm diameter.

deduce the high quality of the Co:BiCuSeO single crystals. One can also see that Co:BiCuSeO has a large valid range for power response. Even when the laser power reached 2mW, the photovoltage did not appear saturation effect. Figure 3(d) shows the photovoltage response under the continuously wavelength-tunable illumination (from 1500 to 1600 nm) near the optical bandgap of the BiCuSeO crystal (~1550 nm). Although the photovoltage is slightly decreased when the wavelength was higher than 1550 nm, there is quite small photoresponse coming from the PC and PV effect. The photovoltage of 4% Co:BiCuSeO crystal was still as large as 0.23 mV even under 1 mW illumination of 1600 nm. Notably, Co:BiCuSeO crystals can be used for broadband photodetection without the limitation of the optical bandgap.

To evaluate the PTE photodetector performance, we extracted the three key figures of merit from above measurement results, i.e., photovoltage responsivity (R), noise equivalent power (NEP), and detectivity (D^*). R is defined as $R = V/P$, where V is the photovoltage induced by laser illumination and P is the laser power incident on the photodetectors. Figure 3(e) depicts the relationship between the responsivity of different doped samples and the illuminating wavelength. There are two features: (1) the wavelength-dependent responsivity trends of different doped samples are quite similar; the responsivity of each sample is strongly dependent on the illuminating wavelength. (2) the 4% Co:BiCuSeO has the largest responsivity among these samples in all measured wavelengths. In what follows, we discuss the physical mechanisms of these two features. Firstly, the responsivity of Co:BiCuSeO is strongly dependent on the illuminating wavelength. Using 4% Co:BiCuSeO as an example, the responsivity is the maximum
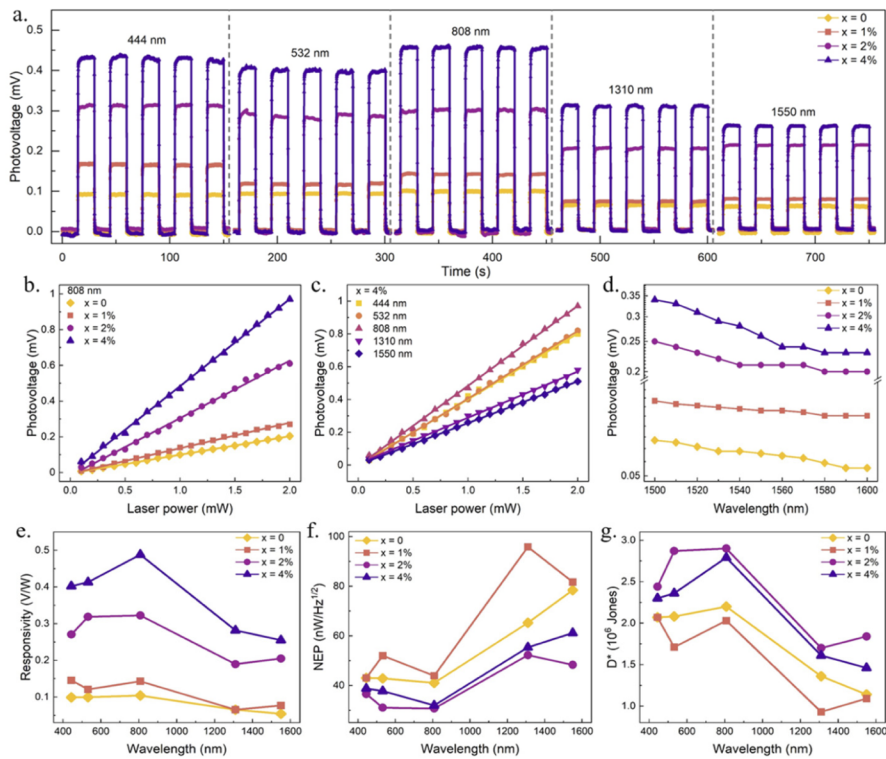
Fig. 3. (a) Wideband time-dependent photovoltage response of Co:BiCuSeO at L-interface across visible to infrared spectral regions. (b) Power-dependence photovoltage response of Co:BiCuSeO under 808 nm. (c) Power-dependence photovoltage response of 4% Co:BiCuSeO under different wavelengths. (d) Photovoltage response under a tunable wavelength region of 1500-1600 nm with fixed power of 1 mW. (e) Calculated responsivity (*R*), (f) noise equivalent power (*NEP*), and (g) detectivity (*D**) at different wavelengths.

as 0.48 V/W under 808 nm laser illumination, which is larger than that under 444 nm illumination (0.40 V/W). In the discussion of Figs. 2(c) and 2(d), we have verified that the photovoltage observed in Co:BiCuSeO comes from the PTE effect, rather than PC or PV effects. To understand the maximum responsivity at 808 nm illumination, we qualitatively discuss this feature through PTE effect. Conceptually, the PTE effect consists of two processes: photo-thermal conversion and thermo-electric conversion. For photo-thermal conversion, electrons absorb the photon energy, and then the extra energy of electrons is transferred to phonon through electron-phonon interaction [31]. In phenomenon, it is manifested as the increase of sample's temperature. More specifically, as shown in Fig. 1(c), the absorption of the same sample is strongly dependent on wavelengths of laser. The pristine and Co-doped BiCuSeO have a maximum absorption around 880 nm illumination. Therefore, it can be inferred that the temperature gradient generated in the same sample at 808 nm illumination is larger than that under 444, 532, 1310 and 1550 nm illuminations. A large temperature gradient, in turn, leads to enhanced photovoltage, as well as responsivity. Therefore, the wavelength-dependent photovoltage response of the same doped sample mainly comes from the difference in light absorption. Secondly, the difference in photovoltage response among the different doped samples under the same wavelength illumination mainly comes from the modification of the Seebeck coefficient by doping. As characterized in Fig. 1(d), 4% Co:BiCuSeO has the largest Seebeck coefficient (962 µV/K). Resultantly, there is the largest responsivity in 4% Co:BiCuSeO. Here, we think there is no significant difference in temperature

gradient for different samples under the same wavelength and the same power laser illumination. This is because the establishment of temperature gradient is closely related to light absorption and thermal conductivity. It can be seen from Fig. 1(c) that the light absorption of the BiCuSeO with different doping is almost the same under the same wavelength of laser illumination. The thermal conductivity of Co:BiCuSeO is quite close to pristine one, which is attributed to thermal conductivity of BiCuSeO mainly coming from the lattice thermal conductivity, while the electron thermal conductivity only contributes the 10% of total thermal conductivity in BiCuSeO as reported in [32].
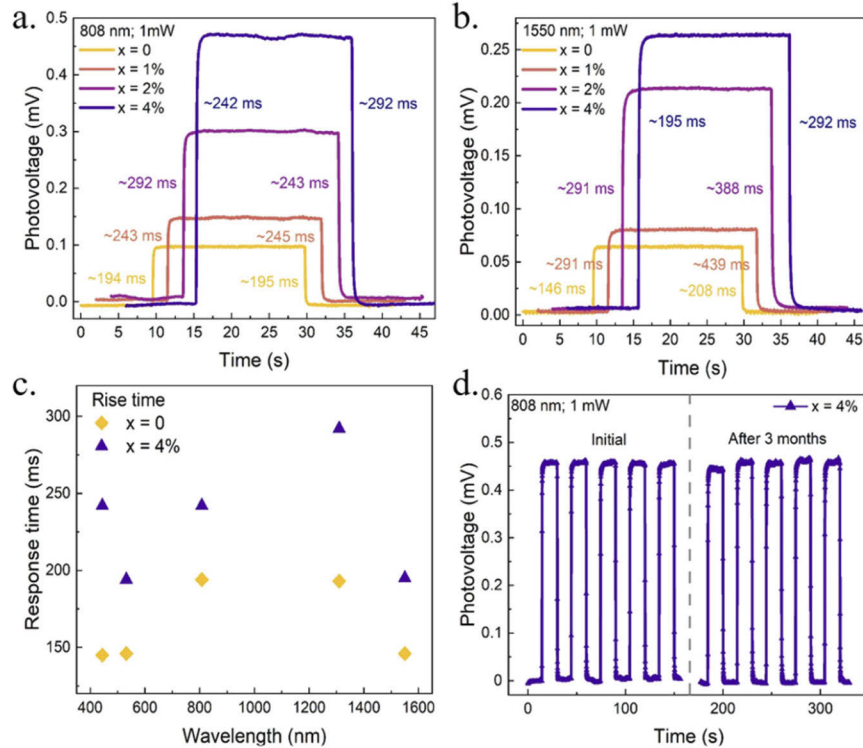

Fig. 4. Rise- and fall-response times of Co:BiCuSeO illuminated at (a) 808 nm and (b) 1550 nm. (c) Comparison of rise response time between pristine BiCuSeO and 4% Co:BiCuSeO under different wavelengths. (d) Stability of time-dependent photovoltage response of 4% Co:BiCuSeO PTE detector after three months.

As shown in Fig. 3(e), it should be emphasized that the responsivities of all Co-doping samples are higher than that of pristine one crossing the entire spectral region. The maximum responsivity (0.48 V/W) in our experiment was realized by 4% Co:BiCuSeO at 808 nm. It is higher than many typical PTE photodetectors as listed in Table 1. The second figure of merit, *NEP*, reflects the minimum detectable illumination power. As previously mentioned, the dark noise of PTE photodetector almost completely comes from Johnson-Nyquist noise. Accordingly, *NEP* can be defined as $NEP = \sqrt{4k_B T R_c}/R$ [7], where k_B is the Boltzmann constant, T = 300 K, R_c is the channel resistance. The calculated *NEP* values in Fig. 3(f) are all below 100 nW/Hz$^{1/2}$ when the wavelength is varied from 444 to 1550 nm, in which 2% Co:BiCuSeO has the minimum *NEP* of 30.7 nW/Hz$^{1/2}$ at 808 nm. The third figure of merit is defined as $D^* = \sqrt{S_A}/NEP$ [30], where S_A is the photosensitive area. As the comparison in Fig. 3(g), the D^* values of all the detectors are higher than 9×10^5 Jones (cm Hz$^{1/2}$ W^{-1}), where with 2% Co:BiCuSeO PTE photodetector having the maximum of 2.9×10^6 Jones at 808 nm.

Table 1. Comparison of performance parameters with typical PTE photodetectors

Active material	Spectral range (nm)	Responsivity (V/W)	Response time (s)	Ref.
Graphene (biased; p-n junction)	457-1550	0.5	-	[35]
Nanoporous silicon	476-514	-	5	[36]
Carbon nanotube (suspended)	544; 685	0.3	0.017	[37]
Bi_2Se_3 nanoribbon	514	2.6	0.7	[15]
SnSe film	405-1550	0.13	3	[14]
SnSe crystal	405-1550	0.07	8	[14]
$SrTiO_3$	325-10600	1.18	1.52	[12]
Photonic crystal (Bi; Ag; TiO_2)	450-720	0.26	3.9	[38]
$MAPbI_3$/reduced graphene oxide film	980-1177	0.044	0.0147	[11]
Thorlabs S350C power detector	190-1100; 10600	0.0013	9	-
4% Co:BiCuSeO single crystal	444-1600	0.48	0.194	**This work**

Considering that the response time is a prominent factor that determines the ability of a photodetector to track the dynamic of an optical signal, we investigated the modulation of Co doping on the response time. The response time, which includes rise time and fall time. The rise (fall) time is defined as the time required for the photovoltage along the rising (falling) edge to increase (decrease) from 10% (90%) to 90% (10%) [12,33]. Figures 4(a) and 4(b) present the temporal photovoltage response of these four photodetectors under 808 and 1550 nm irradiation, respectively. Generally, the long response time is an intrinsic characteristic of PTE photodetectors in which the rise response time of most PTE materials is in the order of seconds, as exhibited in Table 1. Different from this empirical law, all the four devices have relatively short rise and fall times in the range of 100-300 ms albeit there is a slight extension with Co doping. The comparison of rise time between 4% Co-doping and pristine BiCuSeO under different wavelengths is depicted in Fig. 4(c). The rise time of 4% sample is in the range of 194-292 ms somewhat higher than 145-194 ms for the pristine one. These deviations may be attributed to the decrease of the electrical mobility with increasing Co doping level. Quantitatively, the electrical mobilities of un-doped, 1%, 2% and 4% Co:BiCuSeO are 230, 169, 25 and 7 cm^2/(V·s) at low temperature, respectively [29]. Here, it is worthwhile to mention that we used the electrical mobility measured at 10 K to discuss the response time of BiCuSeO, because electron-phonon interaction has little effect on electrical mobility measured at 10 K [34]. The velocity change of electrons under acceleration of laser is so quickly that phonon has no time to response. In addition, it would be more important to note that BiCuSeO has natural advantages in terms of stability as an excellent oxide thermoelectric material. As depicted in Fig. 4(d), the photovoltage response after exposing the 4% device in ambient environment for three months. The response time is still consistent with the initial response, showing an excellent photoresponse stability. As a result, we can conclude that the 4% Co doping sample has the best overall PTE photodetection performance overwhelming the other four samples. Therefore, we believe this work presents a strong case for facilitating the optimization of PTE devices via atomic doping strategy.

3.   Conclusions

In conclusions, here, we systematically characterized the performance of photodetectors made by Co:BiCuSeO crystals under visible and near-infrared spectra. Results substantiate that photovoltage in these photodetectors based on BiCuSeO crystals mainly comes from PTE effect. Co:BiCuSeO PTE photodetectors have better photoresponse performance than pristine one. The enhanced PTE effect in Co:BiCuSeO stems from the increased Seebeck coefficient. Our work suggests that BiCuSeO crystals may be useful in photodetection in some specific environments.

Disclosures. The authors declare no conflict of interest.

Data availability. Data underlying the results presented in this paper are not publicly available at this time but maybe obtained from the authors upon reasonable request.

References

1. X. W. Lu, L. Sun, P. Jiang, and X. H. Bao, "Progress of Photodetectors Based on the Photothermoelectric Effect," Adv. Mater. **31**(50), 1902044 (2019).
2. D. Suzuki, S. Oda, and Y. Kawano, "A flexible and wearable terahertz scanner," Nat. Photonics **10**(12), 809–813 (2016).
3. C. X. Bao, Z. L. Chen, Y. J. Fang, H. T. Wei, Y. H. Deng, X. Xiao, L. L. Li, and J. S. Huang, "Low-Noise and Large-Linear-Dynamic-Range Photodetectors Based on Hybrid-Perovskite Thin-Single-Crystals," Adv. Mater. **29**(39), 1703209 (2017).
4. X. W. He, F. Léonard, and J. Kono, "Uncooled Carbon Nanotube Photodetectors," Adv. Opt. Mater. **3**(8), 989–1011 (2015).
5. J. He and T.M. Tritt, "Advances in thermoelectric materials research: looking back and moving forward," Science **357**(6358), 1369 (2017).
6. H. Chen, C. H. Wang, Z. M. Cheng, L. Y. Wei, F. Q. Wang, and X. X. Zhang, "Performance analysis of a thermoelectric system based on radiative cooling and greenhouse effects," Acta Phys. Sin. **70**(21), 214401 (2021).
7. X. H. Cai, A. B. Sushkov, R. J. Suess, M. M. Jadidi, G. S. Jenkins, L. O. Nyakiti, R. L. Myers-Ward, S. S. Li, J. Yan, D. K. Gaskill, T. E. Murphy, H. D. Drew, and M. S. Fuhrer, "Sensitive room-temperature terahertz detection via the photothermoelectric effect in graphene," Nat. Nanotechnol. **9**(10), 814–819 (2014).
8. M. Buscema, M. Barkelid, V. Zwiller, H. S. J. van der Zant, G. A. Steele, and A. Castellanos-Gomez, "Large and Tunable Photothermoelectric Effect in Single-Layer MoS$_2$," Nano Lett. **13**(2), 358–363 (2013).
9. L. Viti, J. Hu, D. Coquillat, W. Knap, A. Tredicucci, A. Politano, and M. S. Vitiello, "Black Phosphorus Terahertz Photodetectors," Adv. Mater. **27**(37), 5567–5572 (2015).
10. D. J. Groenendijk, M. Buscema, G. A. Steele, S. Michaelis de Vasconcellos, R. Bratschitsch, H. S. J. van der Zant, and A. Castellanos-Gomez, "Photovoltaic and Photothermoelectric Effect in a Double-Gated WSe$_2$ Device," Nano Lett. **14**(10), 5846–5852 (2014).
11. M. Y. Li, X. Tang, S. L. Wang, T. T. Li, J. T. Li, H. L. Zhao, Q. Y. Li, Q. Wang, Y. T. Zhang, and J. Q. Yao, "Synergistic optimization of photothermoelectric performance of a perovskite/graphene composite," Ceram. Int. **48**(3), 4366–4370 (2022).
12. X. W. Lu, P. Jiang, and X. H. Bao, "Phonon-enhanced photothermoelectric effect in SrTiO$_3$ ultra-broadband photodetector," Nat. Commun. **10**(1), 138 (2019).
13. K. W. Mauser, S. Kim, S. Mitrovic, D. Fleischman, R. Pala, K. C. Schwab, and H. A. Atwater, "Resonant thermoelectric nanophotonics," Nat. Nanotechnol. **12**(8), 770–775 (2017).
14. Y. J. Zhong, L. Zhang, V. Linseis, B. C. Qin, W. D. Chen, L. D. Zhao, and H. W. Zhu, "High-quality textured SnSe thin films for self-powered, rapid-response photothermoelectric application," Nano Energy **72**, 104742 (2020).
15. Y. Yan, Z. M. Liao, X. X. Ke, G. V. Tendeloo, Q. S. Wang, D. Sun, W. Yao, S. Y. Zhou, L. Zhang, H. C. Wu, and D. P. Yu, "Topological Surface State Enhanced Photothermoelectric Effect in Bi$_2$Se$_3$ Nanoribbons," Nano Lett. **14**(8), 4389–4394 (2014).
16. T. Winzer, A. Knorr, and E. Malic, "Carrier multiplication in graphene," Nano Lett. **10**(12), 4839–4843 (2010).
17. K. J. Tielrooij, L. Piatkowski, M. Massicotte, A. Woessner, Q. Ma, Y. Lee, K. S. Myhro, C. N. Lau, P. Jarillo-Herrero, N. F. van Hulst, and F. H. L. Koppens, "Generation of photovoltage in graphene on a femtosecond timescale through efficient carrier heating," Nat. Nanotechnol. **10**(5), 437–443 (2015).
18. K. J. Tielrooij, J. C. W. Song, S. A. Jensen, A. Centeno, A. Pesquera, A. Z. Elorza, M. Bonn, L. S. Levitov, and F. H. L. Koppens, "Photoexcitation cascade and multiple hot-carrier generation in graphene," Nat. Phys. **9**(4), 248–252 (2013).
19. X. D. Xu, N. M. Gabor, J. S. Alden, A. M. van der Zande, and P. L. McEuen, "Photo-Thermoelectric Effect at a Graphene Interface Junction," Nano Lett. **10**(2), 562–566 (2010).

20. D. Wang, M. Wright, N. K. Elumalai, and A. Uddin, "Stability of perovskite solar cells," Sol. Energy Mater. Sol. Cells **147**, 255–275 (2016).

21. L. D. Zhao, J. Q. He, D. Berardan, Y. H. Lin, J. F. Li, C. W. Nanc, and N. Dragoe, "BiCuSeO oxyselenides: new promising thermoelectric materials," Energy Environ. Sci. **7**(9), 2900–2924 (2014).

22. G. K. Ren, S. Y. Wang, Z. F. Zhou, X. Li, J. Yang, W. Q. Zhang, Y. H. Lin, J. H. Yang, and C. W. Nan, "Complex electronic structure and compositing effect in high performance thermoelectric BiCuSeO," Nat. Commun. **10**(1), 2814 (2019).

23. X. X. Zhang, C. Chang, Y. M. Zhou, and L. D. Zhao, "BiCuSeO Thermoelectrics: An Update on Recent Progress and Perspective," Materials **10**(2), 198 (2017).

24. G. Y. Yan, L. Wang, S. Qiao, X. L. Wu, S. F. Wang, and G. S. Fu, "Light-induced transverse voltage effect in c-axis inclined BiCuSeO single crystalline thin films," Opt. Mater. Express **6**(2), 558–565 (2016).

25. L. Wang, G. Y. Yan, G. Y. Dong, S. Qiao, G. S. Fu, and S. F. Wang, "Enhanced light-induced transverse thermoelectric effect in c-axis inclined BiCuSeO thin films via Pb doping," Opt. Mater. Express **6**(8), 2537–2544 (2016).

26. L. Y. Wang, G. Y. Yan, S. H. Hou, S. Guo, J. L. Wang, N. Fu, and S. F. Wang, "Temperature-dependent LITT effect in c axis inclined BiCuSeO thin films," Appl. Opt. **57**(12), 3061–3064 (2018).

27. W. Y. Yu, G. Y. Yan, Y. L. Xue, Y. J. Zhang, J. L. Wang, G. S. Fu, and S. F. Wang, "Enhanced Light-Induced Transverse Thermoelectric Effect in Tilted BiCuSeO Film via the Ultra-thin AuNPs Layer," Nanoscale Res Lett **14**(1), 367 (2019).

28. J. Wu, G. Y. Yan, M. J. Chen, Y. L. Xue, L. J. Gao, J. L. Wang, and S. F. Wang, "Enhanced light-induced transverse thermoelectric effect in c-axis inclined Ba-doped BiCuSeO thin films," Appl. Surf. Sci. **570**, 151254 (2021).

29. S. Han, C. H. Yin, Y. Y. Lv, H. M. Lu, Y. C. Luo, L. Xu, S. H. Yao, J. Zhou, and Y. B. Chen, "The electrical- and magneto-transport properties of Rb-, Sn-, and Co-doped BiCuSeO crystals," AIP Adv. **11**(10), 105207 (2021).

30. M. Buscema, J. O. Island, D. J. Groenendijk, S. I. Blanter, G. A. Steele, H. S. J. van der Zant, and A. Castellanos-Gomez, "Photocurrent generation with two-dimensional van der Waals semiconductors," Chem. Soc. Rev. **44**(11), 3691–3718 (2015).

31. W. Schafer and M. Wegener, *Semiconductor Optics and Transport Phenomena* (Springer-Verlag Berlin Heidelberg, 2011).

32. D. J. Lin, S. T. Dong, Y. Y. Zhang, Y. Y. Lv, J. Zhou, Y. B. Chen, R.A. Mole, S. H. Yao, and D. H. Yu, "The physical mechanism of extremely low thermal conductivity of BiCuTeO and BiCuSeO revealed by inelastic neutron and Raman spectroscopy," J. Alloys Compd. **826**, 154161 (2020).

33. W. L. Guo, Z. Dong, Y. J. Xu, C. L. Liu, D. C. Wei, L. B. Zhang, X. Y. Shi, C. Guo, H. Xu, G. Chen, L. Wang, K. Zhang, X. S. Chen, and W. Lu, "Sensitive Terahertz Detection and Imaging Driven by the Photothermoelectric Effect in Ultrashort-Channel Black Phosphorus Devices," Adv. Sci. **7**(5), 1902699 (2020).

34. J. M. Ziman, *Electrons and Phonons: The Theory of Transport Phenomena in Solids* (Oxford University Press, 1960).

35. T. J. Echtermeyer, P. S. Nene, M. Trushin, R. V. Gorbachev, A. L. Eiden, S. Milana, Z. Sun, J. Schliemann, E. Lidorikis, K. S. Novoselov, and A. C. Ferrari, "Photothermoelectric and Photoelectric Contributions to Light Detection in Metal−Graphene−Metal Photodetectors," Nano Lett. **14**(7), 3733–3742 (2014).

36. Y. S. Lai, C. Y. Tsai, C. K. Chang, C. Y. Huang, V. K. S. Hsiao, and Y. O. Su, "Photothermoelectric Effects in Nanoporous Silicon," Adv. Mater. **28**(13), 2644–2648 (2016).

37. B. C. St-Antoine, D. Menard, and R. Martel, "Position Sensitive Photothermoelectric Effect in Suspended Single-Walled Carbon Nanotube Films," Nano Lett. **9**(10), 3503–3508 (2009).

38. H. Monshat, L. J. Liu, and M. Lu, "A Narrowband Photo-Thermoelectric Detector Using Photonic Crystal," Adv. Opt. Mater. **7**(3), 1801248 (2019).